# Magnetic Bearing System for Left Ventricular Assist Artificial Heart Pump – Combined Active and Passive Configuration

Paul Allaire[a], Wei Jiang[b], Arunvel Kailasan[c], Tim Dimond[d]

[a] Rotor Bearing Solutions International, 3277 Arbor Trace, Charlottesville, VA 22911-7580, USA, paul.allaire@rotorsolution.com
[b] University of Virginia, 122 Engineer's Way, Charlottesville, VA 22904, USA
[c] Gardner Denver, Inc., 100 Gardner Park, Peachtree City, GA 30269, USA, arunvel.kailasan@gardnerdenver.com
[d] Rotor Bearing Solutions International, 3277 Arbor Trace, Charlottesville, VA 22911-7580, USA, tim.dimond@rotorsolution.com

***Abstract*—Magnetic bearings continue to contribute to the development of ventricular assist artificial heart pumps. This paper describes the magnetic suspension for a unique prototype axial flow pump designed for approximately 6 l/min at 100 mm Hg performance with an operating speed of approximately 7,000 rpm. The integrated magnetic suspension design provides a direct non-contact blood flow path through the pump with no obstructions which might create low flow areas and thrombosis (blood clots). The magnetic suspension is a combination of permanent magnets (PMs) and active magnetic bearings (AMBs). There are two radial AMBs which support the four degrees of freedom at the ends of the axial pump impeller and an axial PM thrust bearing. The axial PM bearing supports the direction of the largest fluid force on the impeller. A major objectives of artificial hearts is to have extremely low power consumption. Thus the integrated PM and AMB suspension system has an operating magnetic suspension power of approximately 2 watts. The design, numerical modeling, and testing of the magnetic suspension system to support the fluid loads and the g loads is described in the paper.**

## I. INTRODUCTION

The problem of heart disease is a high priority medical research It remains a very significant cause of death or limited capability to live a robust life for many individuals. The number of heart transplants in the United States are severely limited because there are only approximately 2,500 donors per year [1]. Another problem is matching the transplant recipient to the donor. Currently, the use of cyclosporin as an anti-coagulant has made survival on a heart transplant much easier than in the years prior to 1980.

Left ventricular devices (LVADs), designed to support the left ventricle, have proven extremely valuable in use as a bridge to transplant in many patients. In 1994, the US Federal Drug Agency (FDA) approved the first LVAD [1]. The current leader in the field is the Heartmate II, made by Thoratec, a finger sized axial flow pump, approved by the FDA in 2008. The Heartmate II weighs 0.28 kg (10 oz) and requires a sling holding a power module and 3.6 kg (8 lbm) of batteries that require recharging after 8 hours [1]. The unit is plugged into the wall power outlet at night. The current Heartmate II has blood lubricated needle bearings which require recipients to take significant anti-coagulation medication. Another popular LVAD is made by Heartware International [1]. In 2012, about 2,000 LVADs were implanted, as compared to 200 in 2006 [1]. As many as 40% of LVADs are now categorized as destination therapy or permanent assist devices. It is noted that the future likely holds magnetic suspension for LVADs, according to Thoratec officials [1].

The first LVAD configuration utilizing an active magnetic suspension in a centrifugal pump, including a 90 day animal implant, was reported in a number of publications in the mid-1990s [2,3]. It used a full electromagnetic suspension but this type of suspension produced high currents and too much heat. The next centrifugal pump utilizing a magnetic suspension employed permanent magnets in combination with the electromagnets, called a hybrid system, greatly reduced the coil currents [4-12, 16]. There is no method of supporting a body solely with permanent magnets so at least one axis must be actively controlled, as proven in Earnshaw's theorem. The axis along the centrifugal impeller axis was actively controlled. This pump configuration eventually was tested in animal and human tests and produced for clinical use by World Heart under the title Levacor. Manufacture of this device ceased in 2011.

The surgeons associated with the development of the Levacor LVAD desired an axial flow pump which would be more suited for implantation. An axial flow LVAD design, called the Lifeflow LVAD, formulated in the late 2000s, was developed with a combined active/permanent magnet system that is reported in this paper. The basis for the permanent magnet design was originally developed in [13,14]. A general paper on sliding mode control of active magnetic bearings related to heart pumps was developed in [15]. An initial paper on this new axial flow suspension, in the Lifeflow LVAD pump, was written in 2007 [17]. The major objective of the suspension was to support the impeller when subject to blood flow forces due to the flow in the pump with a minimum of power consumption, yet be capable of preventing contact between the impeller and LVAD housing when subject to an 8 g dynamic load in any direction. The Lifeflow magnetic suspension, described in this paper, consists of a

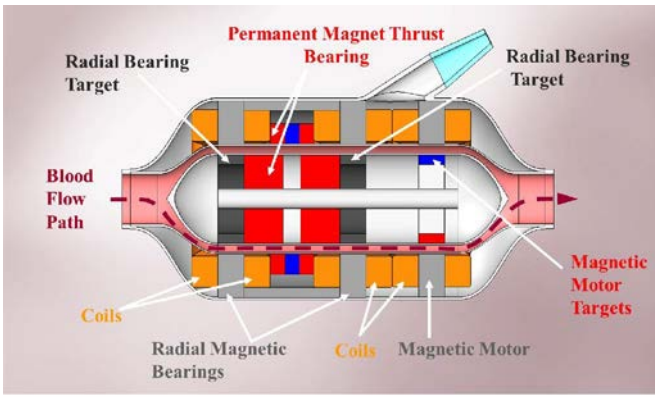


Figure 1. Cutaway View of Lifeflow LVAD Configuration

permanent magnetic axial bearing and two radial active magnetic bearings with permanent magnet bias. The measured power consumption in a suspension test rig was 2 watts when operated at 7,000 rpm.

## II. MAGNETIC SUSPENSION SYSTEM

A cutaway view of the LVAD is shown in Fig. 1. The bloodflow path is a direct, unobstructed flow path around the pump axial impeller, which has a series of spiral vanes on the outer diameter. It has a flow rate of 3 to 8 l/min with a design flow of approximately 6 l/min at 7,000 rpm. The hybrid 5 axis magnetic suspension system for the LVAD consists of a combination of PM magnet bearings and active magnetic bearings (AMBs), as illustrated in Fig. 1. Figure 2 shows another, more detailed view of the pump and the magnetic bearing system.

A perspective view of the magnetic suspension stator design for this LVAD is shown in Fig. 3, a stator length of 0.03 m.. The rotor outer diameter is 8 mm and the stator inner diameter is 10 mm with an airgap of 2 mm. Included in the airgap will be the titanium canning material. The highest loads on the pump impeller are due to the pressure difference across the pump. The axial axis PM generates a positive PM stiffness k_z, which places the impeller in the axial center of the clearance space inside the impeller housing. The radial bearings are AMBs, both front and back inside the housing clearance. The AMBs and back iron are made with cobalt iron laminations. The physical magnetic suspension system stator prototype is shown in Fig. 4. The silver components are the permanent magnets while the coils and darker AMB lamination stacks of the two radial bearings are clearly shown. The magnetic suspension test rig for operating the motor and magnetic suspension is shown in Fig. 5. Also, the Lifeflow rotor with magnetic components in the center for both radial AMB lamination stacks and PMs. Steel shaft ends were added for displacement sensors in the testing.

The two radial bearings are each six pole AMBs, as illustrated in Fig. 6, with an equal number of wire turns on each magnetic pole. The pole face area for each pole is 41.4 sq mm. The laminations were constructed of M-19 steel. The backiron allows for magnetic communication between the poles.

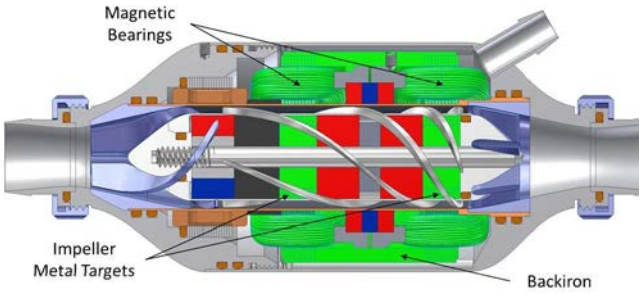


Figure 2. Lifeflow pump schematic showing flow path and magnetic bearings

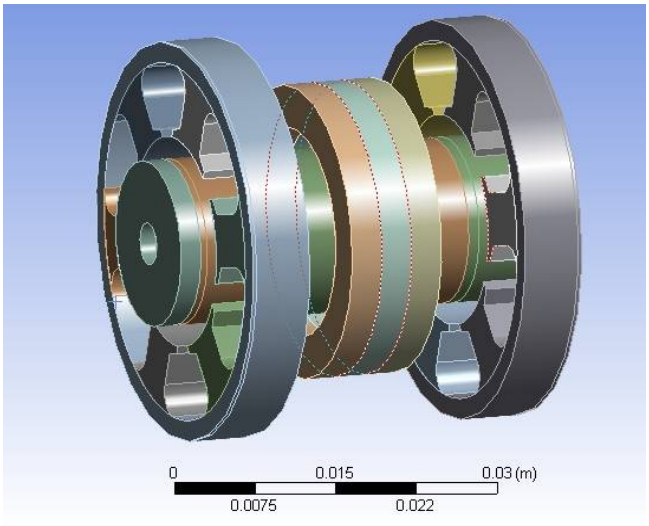


Figure 3. Perspective view of the bearing stator structure

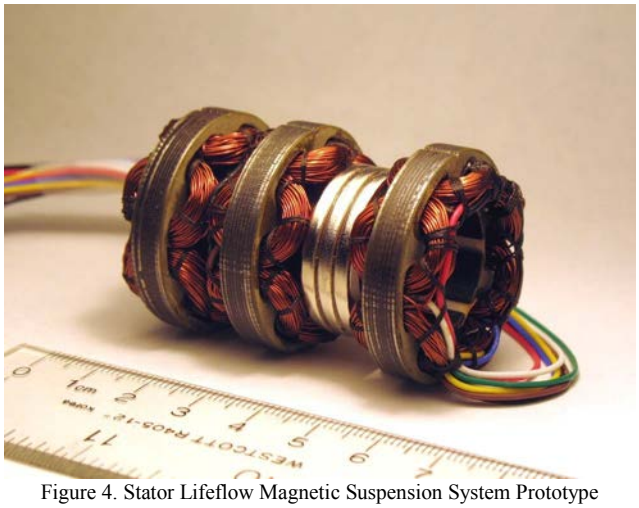

Figure 4. Stator Lifeflow Magnetic Suspension System Prototype

It is well known that the way to reduce the coil power consumption is to supply the bias flux using a permanent magnet flux. The hybrid configuration shown in Fig. 5 uses the PM and AMB flux paths in a way to generate the combined radial flux which add the PM flux in the rotor to the two radial bearing active flux magnitude when they go through the radial bearings. The AMB M-19 iron has a linear operation value near 1.3 T and a saturation flux near

Figure 5. Magnetic Suspension Test Rig and Lifeflow LVAD Magnetic Suspension Rotor Component

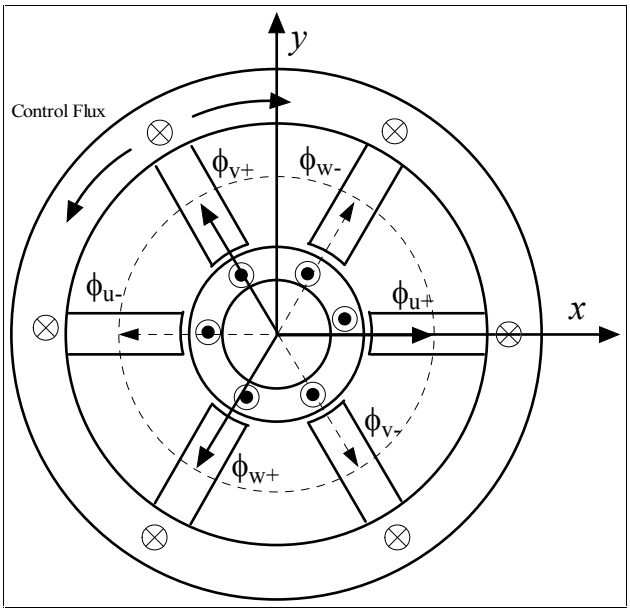


Figure 6. Active Magnetic Bearing Flux in Six Poles

2.0 T, so the PM bias flux is set at approximately half of that or 0.6 T. The coils were selected to provide the magneto-motive force NI to attain the remaining airgap flux density near the linear limit of approximately 1.3 T.

The PM flux path requires a high flux level which is not attainable with a simple PM circuit design. The three PM components in the stator (housing) part of the are configured in the reverse polarity way, as shown in Fig. 1, such that the polarities are 1) S-N (shown in the left red block), 2) N-S (shown in the center blue block), and 3) S-N (shown in the right red block). This special configuration gives a much higher flux density level than a simple, single set of PMs. In the rotor, two simple PMs are placed as shown in Fig. 1 (as shown in the two red blocks). These rotor PMs have two purposes: first, supply the PM bias flux for the radial bearings and second, axial stiffness desired to keep the impeller centered when it is subject to the applied fluid load. The PM material was NdFeB 35 EH.

A three dimensional finite element model of the six pole active magnetic bearing structure is shown in Fig. 7. The rotor three dimensional finite element model is shown in Fig. 8.

A 3-D finite element analysis of the combined AMB-PM system without control currents using ANSYS was also formulated. Figure 9 shows an example of the three dimensional flux plot including both active and passive magnetic suspension system. Also, Fig. 10 shows an example side view of the three dimensional plot. This analysis was used to determine the positive open loop axial stiffness with the result of $k_z$ = 8,65 N/mm, as shown in Fig. 11. The negative open loop radial stiffness, also without coil currents was $k_x$ = - 17.65 N/mm. When coil currents are added, the linearized radial current gain was $k_i$ = 0.688 N/A to be used in controlling the magnetic suspension system. Figure 12 shows the plot of force vs. coil current. The finite element flux levels in the radial air gaps were found to be in the range of 0.31 to 0.36 Tesla.

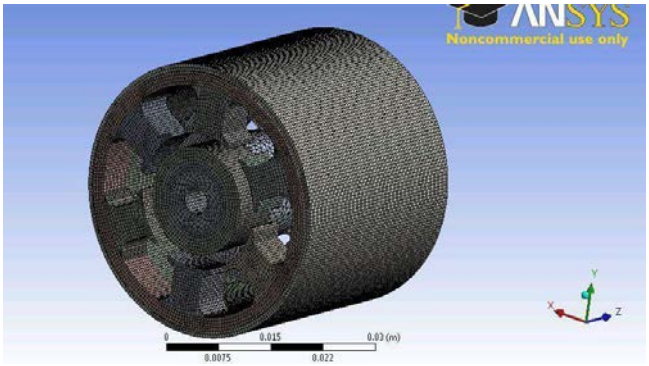


Figure 7. Three dimensional finite element model of the six pole active laminated magnetic bearing structure

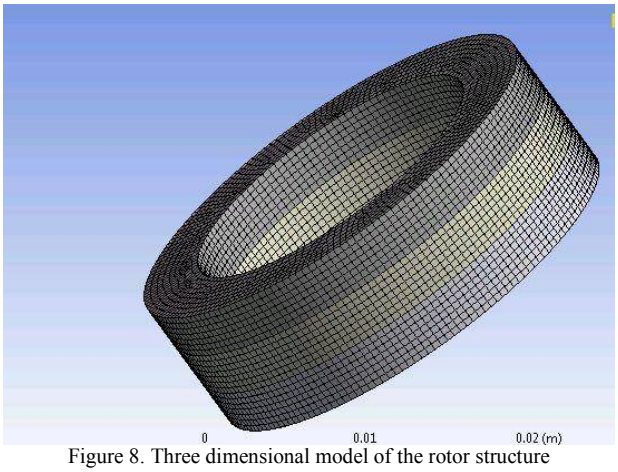


Figure 8. Three dimensional model of the rotor structure in the active magnetic bearing components

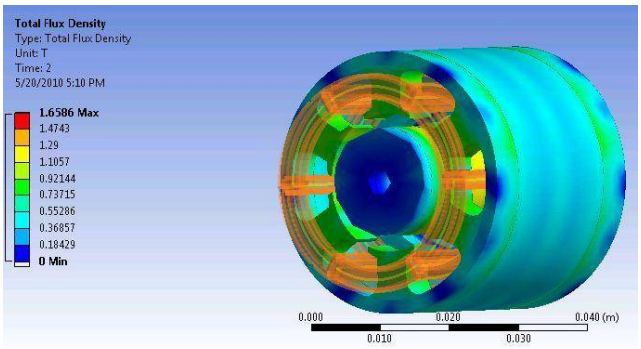


Figure 9. Perspective view of three dimensional flux density plot in the combined active and passive magnetic suspension system.

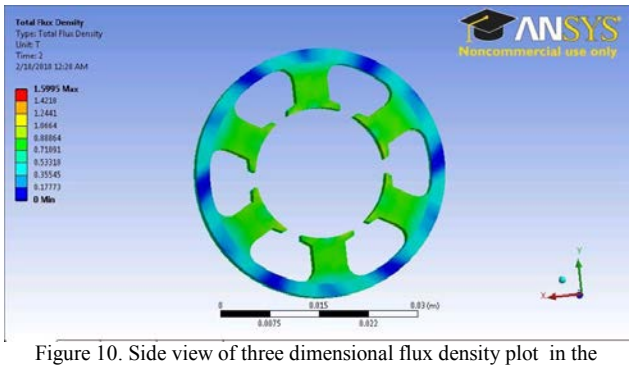


Figure 10. Side view of three dimensional flux density plot in the combined active and passive magnetic suspension system.

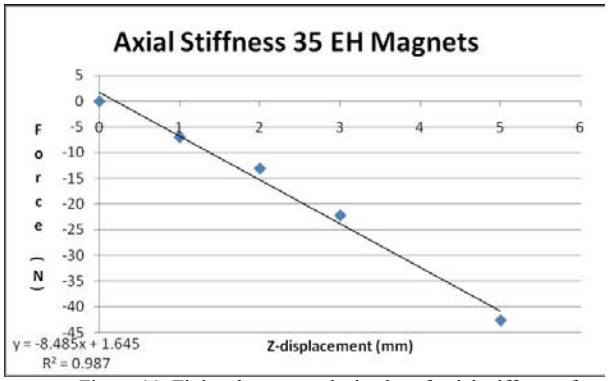


Figure 11. Finite element analysis plot of axial stiffness of combined acive and passive magnetic suspension system

It is also important to evaluate the influence of the blood flow on the rotor. These values were obtained using computational fluid dynamics where the impeller was calculated in the centered position and then moved radially a small distance [18]. The calculation was performed in the rotating coordinate system and then transformed into the fixed coordinate system. The effective radial stiffness is $k_{xx}$ = -5.9 N/mm, $k_{xy}$ = 7.3 N/mm, $k_{yx}$ = -9.1 N/mm, and $k_{yy}$ = -6.5 N/mm at 7,000 rpm. The effective radial damping is $c_{xx}$ = $5.7\cdot10^{-4}$ N-s/mm, $c_{xy}$ = $3.68\cdot10^{-4}$ N-s/mm, $c_{yx}$ = $-3.28\cdot10^{-4}$ N-s/mm, and $c_{yy}$ = $2.2\cdot10^{-4}$ N-s/mm also at 7,000 rpm. The added mass terms are $m_{xx}$ = $0.72\cdot10^{-4}$ N-s$^2$/mm, $m_{xy}$ = $0.09\cdot10^{-4}$ N-s$^2$/mm, $m_{yx}$ = $-0.29\cdot10^{-4}$ N-s$^2$/mm, and $m_{yy}$ = $0.79\cdot10_{-4}$ N-s$^2$/mm.

## III. Magnetic Circuit Model

The control of the radial AMB axes was carried out with a magnetic flux circuit model. The magnetic flux simple circuit model is shown in Fig. 13 with both the AMB and PM circuits included. The magneto-motive force relations for the six pole radial bearings are given by:

$$\begin{aligned}&\phi_{u+}R_{u+} - NI_u = \phi_{u-}R_{u-} + NI_u \\ &= \phi_v + R_{v+} - NI_v = \phi_{v-}R_{v-} + NI_v \\ &= \phi_{w+}R_{w+} - NI_w = \phi_{w-}R_{w-} + NI_w\end{aligned} \tag{1}$$

There are three control current components, after taking the opposite poles as employing paired components of the system. The flux constraint equation is

$$\phi_{u+} + \phi_{u-} + \phi_{v+} + \phi_{v-} + \phi_{w+} + \phi_{w-} = \phi_0 \tag{2}$$

The air gap reluctances for the six poles are given in the following set of equations

$$\begin{aligned}R_{u+} &= \frac{g_0}{\mu_0 A}(1-x) \\ R_{u-} &= \frac{g_0}{\mu_0 A}(1+x) \\ R_{v+} &= \frac{g_0}{\mu_0 A}\left(1+\frac{x}{2}-\frac{\sqrt{3}y}{2}\right) \\ R_{v-} &= \frac{g_0}{\mu_0 A}\left(1-\frac{x}{2}+\frac{\sqrt{3}y}{2}\right) \\ R_{w+} &= \frac{g_0}{\mu_0 A}\left(1+\frac{x}{2}+\frac{\sqrt{3}y}{2}\right) \\ R_{w-} &= \frac{g_0}{\mu_0 A}\left(1-\frac{x}{2}-\frac{\sqrt{3}y}{2}\right)\end{aligned} \tag{3}$$

Assembling all of these equations into matrix form yields the AMB control matrix in the form, involving the pole flux variables, as shown in the Appendix. This is a rather large matrix system of size 6x6 that needs to be reduced for efficient control operation.

### A. System Size Reduction

The controller must be placed in a small controller space, on single circuit board, in the on-body LVAD controller box**.** A smaller order control system matrix will be more compact and simplify the circuit board design and construction. We

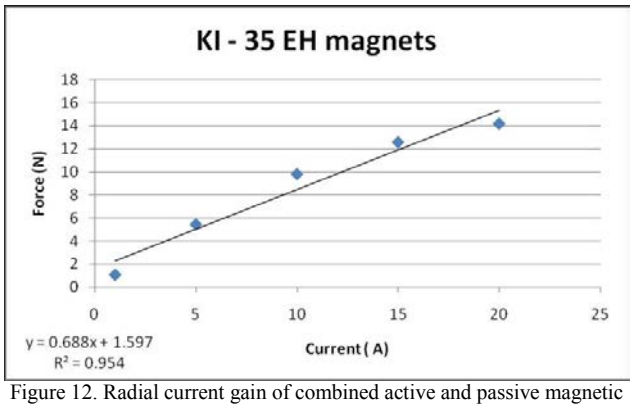

Figure 12. Radial current gain of combined active and passive magnetic bearing system evaluated with three dimensional finite elements.

introduce a combination of the basic flux variables of the form:

$$\begin{aligned}
\phi_{us} &= \phi_{u+} - \phi_{u-} \\
\phi_{ua} &= \phi_{u+} + \phi_{u-} \\
\phi_{vs} &= \phi_{v+} - \phi_{v-} \\
\phi_{vm} &= \phi_{v+} + \phi_{v-} \\
\phi_{ws} &= \phi_{w+} - \phi_{w-} \\
\phi_{wa} &= \phi_{w+} - \phi_{w-}
\end{aligned} \tag{4}$$

We assume that the rotor radial displacements x, y are small compared to the radial clearance between the rotor surface and the housing. Thus, second order terms in the approximation are neglected. Then, the system control matrix equations reduce to the form shown in the Appendix.

The force equations have the form

$$\begin{aligned}
F_u &= \left(\phi_{u+}^2 - \phi_{u-}^2\right)\frac{1}{2\mu_0 A} = \phi_{us}\phi_{ua}\frac{1}{2\mu_0 A} \\
F_v &= \left(\phi_{v+}^2 - \phi_{v-}^2\right)\frac{1}{2\mu_0 A} = \phi_{vs}\phi_{va}\frac{1}{2\mu_0 A} \\
F_w &= \left(\phi_{w+}^2 - \phi_{w-}^2\right)\frac{1}{2\mu_0 A} = \phi_{ws}\phi_{wa}\frac{1}{2\mu_0 A} \\
F_x &= F_u - \frac{1}{2}F_v - \frac{1}{2}F_w \\
F_y &= \frac{\sqrt{3}}{2}F_v - \frac{\sqrt{3}}{2}F_w
\end{aligned} \tag{5}$$

Here the first three relations in Eq. (5) give the net forces in the three primary pole axes in the three pole pair axes. The next two force equations give the force components in the $x$, $y$ coordinate directions. The combined flux variables in the first three force equations above are related to the control currents via the relations:

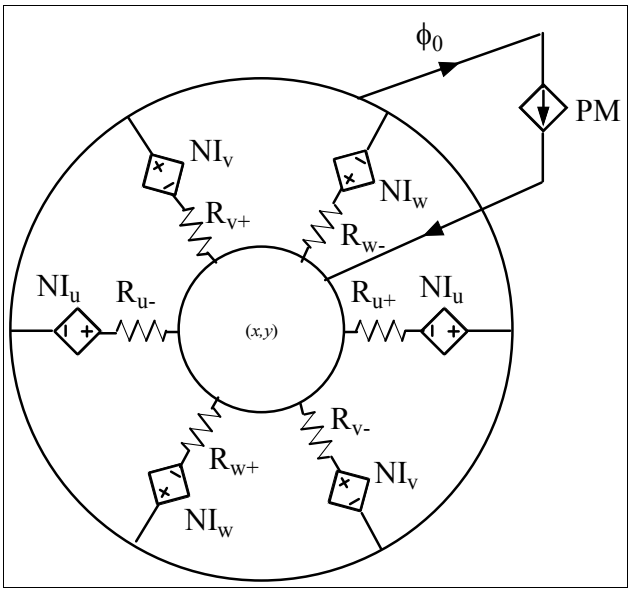

Figure 13. Simple circuit model to calculate flux

$$\begin{aligned}
\phi_{us} &= 2\frac{\mu_0 NA}{g_0}I_u + x\frac{\phi_0}{3} \\
\phi_{ua} &= \frac{\mu_0 NA}{g_0}\left(\frac{4x}{3}I_u + \frac{x-\sqrt{3}y}{3}I_v + \frac{x+\sqrt{3}y}{3}I_w\right) + \frac{\phi_0}{3}
\end{aligned} \tag{6}$$

The values of the AMB and PM fluxes are indicated above to obtain the PM flux level at approximately 0.6 T and the AMB maximum flux level also equal to 0.6 T.

A simple PID controller was used for the control of the radial bearings. Non contact displacement sensors were used in the test rig for levitation testing. Various values for the PID control were tested. Operation above 8,000 rpm was attained. In the final pump, it was intended that a self sensing system, as reported in [17], was used for feedback control.

With this configuration, a sudden load to one side of the impeller is calculated to withstand a g load of 8 based upon the mass of the impeller, the maximum available control current and the reduced order control matrix. It may be noted that a patient with an LVAD falling flat on the ground would produce a load of approximately 2$g$. Thus, the design for 8$g$ should provide an excellent margin of safety for impact loading on the magnetic suspension.

## IV. CONCLUSIONS

This paper describes a new hybrid magnetic suspension designed for an axial flow left ventricular assist device. It has a combined active and passive magnetic bearing which minimizes the power consumption of the suspension system with a measured power loss, in the test rig described above, of 2 watts when operating centered in the clearance space at 7,000 rpm. When compared to the calculated motor power of 10 watts when operating with blood flow, this is quite a small value.

A 3-D magnetic finite element model was developed to evaluate the open loop stiffness and current gain values. Also, the effective stiffness, damping and added mass terms were added to the AMB controller model. It should be noted that the blood flow radial stiffness values are of similar magnitude of the magnetic open loop stiffness.

The method of developing the control system matrix based upon the basic pole flux values was developed. However it was rather large in size. A new method of control using a combination of pole flux values was developed. It resulted in a reduced control matrix for easier implementation in a single circuit board controller suitable for a wearable LVAD. The magnetic suspension was constructed and operated in a test rig. Also, the small operating power of the magnetic suspension will likely increase battery life with a single charge. Unfortunately, the complete pump with blood flow and magnetic suspension was never built due to lack of funds.

## AUTHOR'S NOTE

The authors are grateful for the funding provided for this project through the ROMAC Industrial Research Program under the Direction of Prof. Paul Allaire.

## REFERENCES

[1] A. Allen, "Heart to Heart", *Washington Post,* 2013

[2] P. E. Allaire, H. C. Kim, E. H. Maslen, G. B. Bearnson, and D. B. Olsen, "Design of a Magnetic Bearing Supported Prototype Centrifugal Artificial Heart Pump," *Tribology Transactions*, vol. 39, no. 3, pp. 663–669, 1996.

[3] G. B. Bearnson, E. H. Maslen, D. B. Olsen, P. E. Allaire, P. S. Khanwilkar, J. W. Long, and I. C. Kim, "A proposal and trial on a model of a motion monitor system for a ski jumper using terrestrial magnetism and acceleration sensors," *Journal of American Society of Artificial Internal Organs*, vol. 20, no. 3, pp. 275–281, 1996.

[4] P. Khanwilkar, D. Olsen, G. Bearnson, P. Allaire, E. Maslen, R. Flack, and J. Long, "Using Hybrid Magnetic Bearings to Completely Suspend the Impeller of a Ventricular Assist Device," *Artificial Organs*, vol. 20, no. 6, pp. 597–604, 1996.

[5] E. Hilton, P. Allaire. M. Baloh, E. Maslen, G. Bearnson, P. Khanwilkar, and D. Olsen, "Magnetic suspension controls for continuous flow ventricular assist device," *ASAIO Journal*, vol. 43, no. 5, pp. M598–M602, 1997.

[6] P. Allaire, G. Bearnson, R. Flack, E. Maslen, M. Baloh, E. Hilton, D. Baun, D. Noh, P. Khanwilkar, D. Olsen, A. Goshorn, and T. Waters, "Continuous Flow Magnetically Suspended Centrifugal Flow Pump For Ventricular Assist Device (CFVADIII): Design and Testing," *Artificial Organs*, vol. 22, no. 6, pp. 475–480, 1996.

[7] Y. Nose, T. Tsutsui, K. Butler, R. Jarvik, Y. Takami, C. Nojiri, P. Allaire, O. Van Ram, and J. Dow, "Rotary Pumps – New Developments & Future Perspectives," *ASAIO Journal*, vol. 44, no. 3, pp. 234–237, 1998.

[8] G. Bearnson, D. Olsen, P. Khanwilkar, J. Long, M. Sinnott, A. Kumar, P. Allaire, M. Baloh, and J. Decker, "An Implantable Centrifugal Pump with Hybrid Magnetic Bearings," *ASAIO Journal*, vol. 44, no. 5, pp. M733–M736, 1998.

[9] M. J. Baloh, P. E. Allaire, E. F. Hilton, N. Wei, E. H. Maslen, D. Baun, R. D. Flack, D. B. Olsen, G. B. Bearnson, and P. Khanwilkar, "Magnetic Bearign System for Continuous Flow Ventricular Assist Device," *Artifical Organs Journal*, vol. 45, no. 5, 1998.

[10] M. J. Baloh, P. E. Allaire, E. F. Hilton, N. Wei, D. Baun, R.. Flack, G. B. Bearnson, D. B. Olsen, and P. Khanwilkar, "Characterization of a Magnetic Bearing System and Fluid Properties for a Continuous Flow Ventricualar Assist Device," *Artifical Organs*, vol. 23, no. 8, pp. 792-796, 1999.

[11] P. E. Allaire, J. Decker, M. Baloh, J. Lee, and J. Long, "Magnetic Suspension of an Artificial Heart Pump Using EM/PM Bearings," *Proceedings of the NASA Fifth International Conference on Magnetic Suspension Technology*, 1999.

[12] S. M. Fiser, H. G. Wood, P. E. Allaire, J. M. Long, A. K. Kaza, I. L. Kron, J. A. Kern, and C. G. Tribble, "A Long Term Ventricular Assist Device Utilizing Magnetic Bearing System and Implantable Controller," *Heart Surgery Forum*, vol. 4, no. 1, pp.11-12, 2001.

[13] W. Jiang, P. E. Allaire, M. Baloh, and H. G. Wood, "Magnetic Vector Potential Analysis of Permanent Magnet Suspension System: Forces and Moments," *Proceedings of the Eighth International Symposium on Magnetic Bearings*, pp. 521-525, 2002.

[14] W. Jiang, P. E. Allaire, M. Baloh, and H. G. Wood, "Analysis of Permanent Magnet Suspension System: Stiffness and Stability," *Proceedings of the Eighth International Symposium on Magnetic Bearings*, pp. 527-532, 2002.

[15] J. H. Lee, P. E. Allaire, G. Tao, and J. A. Decker, "Experimental Study of Sliding Mode Control for a Benchmark Magnetic Bearing System and Artifical Heart Pump Suspension," *IEEE Transactions on Control Systems Technology*, vol. 11, no. 1, pp. 128-138, 2003.

[16] X. Song, W. Jiang, H. G. Wood, P. E. Allaire, and D. B. Olsen, "Numerical Analysis for Off-center Performance of Magnetic Bearings," *30th Annual Conference of European Society for Artifical Organs*, 2003.

[17] P. E. Allaire and W. Jiang, "Design and Testing of the Lifeflow Total Magnetic Suspension Left Ventricular Assist Device," *15th Congress of International Society of Rotary Blood Pumps*, 2007.

[18] A. Untariou, H. G. Wood, P. E. Allaire and T. W. Dimond, "Calculation of Dynamic Coeficients for a Magnetically Levitated Artifical Heart Pump Using CFD Approach," *Proceedings of the ASME International Mechanical Engineering Conference*, 2008.

## APPENDIX: RADIAL BEARING CONTROL MATRICES

The large control matrix for the radial bearings in terms of the basic pole flux variables and control currents is

$$\begin{bmatrix} 1-x & -1-x & 0 & 0 & 0 & 0 \\ 0 & 1+x & -1-\frac{x}{2}+\frac{\sqrt{3}y}{2} & 0 & 0 & 0 \\ 0 & 0 & 1+\frac{x}{2}-\frac{\sqrt{3}y}{2} & -1+\frac{x}{2}-\frac{\sqrt{3}y}{2} & 0 & 0 \\ 0 & 0 & 0 & 1-\frac{x}{2}+\frac{\sqrt{3}y}{2} & -1-\frac{x}{2}-\frac{\sqrt{3}y}{2} & 0 \\ 0 & 0 & 0 & 0 & 1+\frac{x}{2}+\frac{\sqrt{3}y}{2} & -1+\frac{x}{2}+\frac{\sqrt{3}y}{2} \\ 1 & 1 & 1 & 1 & 1 & 1 \end{bmatrix} \begin{Bmatrix} \phi_{u+} \\ \phi_{u-} \\ \phi_{v+} \\ \phi_{v-} \\ \phi_{w+} \\ \phi_{w-} \end{Bmatrix} = \begin{bmatrix} 2 & 0 & 0 \\ -1 & -1 & 0 \\ 0 & 2 & 0 \\ 0 & -1 & -1 \\ 0 & 0 & 2 \\ 0 & 0 & 0 \end{bmatrix} \frac{\mu_0 NA}{g_0} + \begin{Bmatrix} 0 \\ 0 \\ 0 \\ 0 \\ 0 \\ \phi_0 \end{Bmatrix} \quad (7)$$

in terms of the pole geometry, basic pole flux values, pole axis control currents, and the permanent magnet flux value. The reduced radial bearing control matrix in terms of combined flux variables, control currents, and permanent magnetic flux value is given by

$$\begin{Bmatrix} \phi_{us} \\ \phi_{ua} \\ \phi_{vs} \\ \phi_{va} \\ \phi_{ws} \\ \phi_{wa} \end{Bmatrix} = \frac{\mu_0 NA}{g_0} \begin{bmatrix} 2 & 0 & 0 \\ \frac{4x}{3} & \frac{x-\sqrt{3}y}{3} & \frac{x+\sqrt{3}y}{3} \\ 0 & 2 & 0 \\ -\frac{2x}{3} & \frac{-2x+2\sqrt{3}y}{3} & \frac{x+\sqrt{3}y}{3} \\ 0 & 0 & 2 \\ -\frac{2x}{3} & \frac{x-\sqrt{3}y}{3} & \frac{-2x-2\sqrt{3}y}{3} \end{bmatrix} \begin{Bmatrix} I_u \\ I_v \\ I_w \end{Bmatrix} + \frac{\phi_0}{6} \begin{Bmatrix} 2x \\ 2 \\ -x+\sqrt{3}y \\ 2 \\ -x-\sqrt{3}y \\ 2 \end{Bmatrix} \quad (8)$$

This is much smaller and more suitable for a single circuit board controller.